Validation of model-based deformation correction in image-guided liver surgery via tracked intraoperative ultrasound: preliminary method and results

Logan W. Clements[a], Jarrod A. Collins[a], Yifei Wu[a], Amber L. Simpson[b], William R. Jarnagin[b], and Michael I. Miga[a,c,d]

[a]Vanderbilt University, Dept. of Biomedical Engineering, Nashville, TN
[b]Memorial Sloan-Kettering Cancer Center, Dept. of Surgery, New York, NY
[c]Vanderbilt University, Dept. of Radiology and Radiological Sciences, Nashville, TN
[d]Vanderbilt University, Dept. of Neurological Surgery, Nashville, TN

ABSTRACT

Soft tissue deformation represents a significant error source in current surgical navigation systems used for open hepatic procedures. While numerous algorithms have been proposed to rectify the tissue deformation that is encountered during open liver surgery, clinical validation of the proposed methods has been limited to surface based metrics and sub-surface validation has largely been performed via phantom experiments. Tracked intraoperative ultrasound (iUS) provides a means to digitize sub-surface anatomical landmarks during clinical procedures. The proposed method involves the validation of a deformation correction algorithm for open hepatic image-guided surgery systems via sub-surface targets digitized with tracked iUS. Intraoperative surface digitizations were acquired via a laser range scanner and an optically tracked stylus for the purposes of computing the physical-to-image space registration within the guidance system and for use in retrospective deformation correction. Upon completion of surface digitization, the organ was interrogated with a tracked iUS transducer where the iUS images and corresponding tracked locations were recorded. After the procedure, the clinician reviewed the iUS images to delineate contours of anatomical target features for use in the validation procedure. Mean closest point distances between the feature contours delineated in the iUS images and corresponding 3-D anatomical model generated from the preoperative tomograms were computed to quantify the extent to which the deformation correction algorithm improved registration accuracy. The preliminary results for two patients indicate that the deformation correction method resulted in a reduction in target error of approximately 50%.

Keywords: clinical validation, biomechanical modeling, image-guided surgery, open liver surgery, soft tissue deformation, tracked ultrasound

1. INTRODUCTION

Similar to the well documented brain shift experienced during neurosurgical procedures, intra-operative soft tissue deformation in open hepatic resections is the primary source of error in current image-guided liver surgery (IGLS) systems. A number of studies have performed measurements via intraoperative imaging to quantify the extent of deformation. A study by Heizmann *et al.* used intraoperative computed tomography (iCT) to visualize soft tissue deformation via rendered vascular structures and to quantify volumetric changes in anatomical regions during the surgical procedure.[1] Work presented by Cash *et al.* highlighted a preliminary summary of the incidence of soft tissue deformation during IGLS procedures.[2] Additionally, our previous work has focused on quantifying surface deformations during open hepatic surgery using laser range scan (LRS) surface acquisitions of the anterior

Correspondence:
Logan W. Clements
Department of Biomedical Engineering
Vanderbilt University
P.O. Box 351631, Station B
Nashville, TN 37235
logan.clements@vanderbilt.edu

organ surface.[3] Figure 1 highlights a series of renderings of the signed closest point distance maps between the LRS surfaces acquired during the procedure and 3-D organ surfaces generated from the preoperative tomograms for three patients that underwent biopsies and resections in the right lobe.
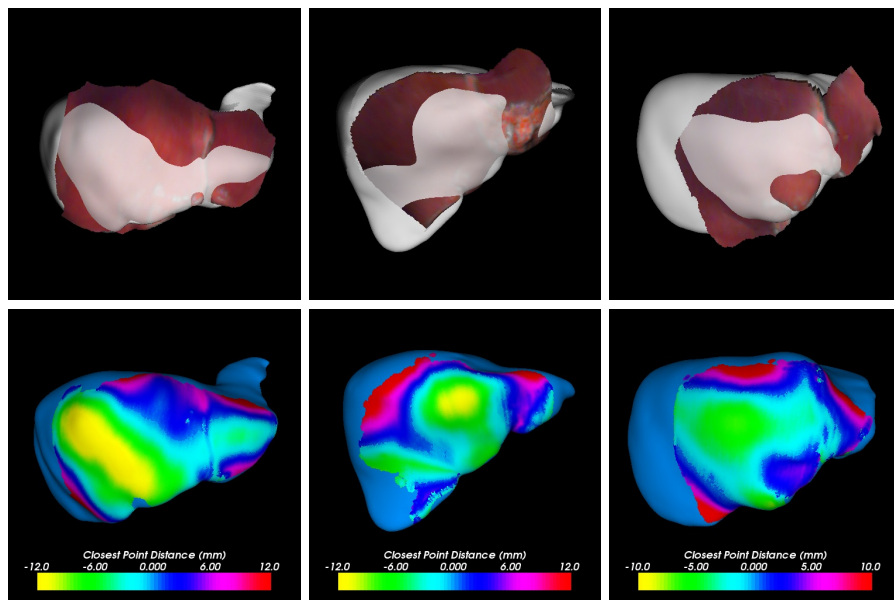

Figure 1. Figures showing the results of salient feature surface registration and the corresponding signed closest point distance maps for three clinical patients undergoing biopsy or resection procedures in the right lobe (published in Clements *et al.*[3]). The three sets of data demonstrate the incidence of significant soft tissue deformation in open IGLS. In some areas, closest point distance measurements are nearly 2 cm.

Given the fact that intraoperative soft tissue deformation can limit the utility of preoperative tomographic imaging for surgical guidance, numerous avenues have been suggested to aid in the compensation for the experienced soft tissue deformation, including the use of intraoperative tomography and ultrasound. However, intraoperative magnetic resonance (iMR) and iCT imaging equipment is cumbersome, overly expensive for a majority of hospital budgets, and not presently considered standard of care in open liver procedures. Additionally, intraoperative 2-D ultrasound (iUS) provides low signal-to-noise, sparse images of the patient's anatomy. Studies have been performed to evaluate the utility of 3-D iUS for navigated resection of liver tumors, but such a system is limited by the fact that some lesions can not be identified via iUS imaging.[4] Ultimately, the ideal image-guidance modality is to update the high contrast, high resolution preoperative tomograms to match the intraoperative presentation.

1.1. Objective

The primary objective of this work is to define a validation procedure of a model-based deformation compensation algorithm driven by sparse organ surface data using tracked iUS acquisitions of sub-surface anatomical landmarks acquired during clinical procedures. A sub-surface target error metric can be computed between the contour of anatomical structures delineated in tracked iUS and corresponding 3-D anatomical models generated from preoperative image sets.

2. METHODS

The proposed deformation correction clinical validation technique involves three steps: (1) clinical data collection using a surgical navigation system equipped with ultrasound tracking functionality, (2) retrospective deformation

correction using the intraoperatively acquired liver surface digitization to drive the algorithm, and (3) retrospective quantification of the efficacy of deformation correction based on sub-surface anatomical landmarks that can be localized in the tracked iUS images as well as the preoperative tomograms.

2.1. Clinical Data Collection

For this preliminary study, a series of clinical data has been acquired for four patients undergoing open liver resection at Memorial Sloan-Kettering Cancer Center. The four patients provided written consent and were enrolled in an ongoing study that has been approved by the Memorial Sloan-Kettering Institutional Review Board.

2.1.1. Preoperative Image Processing

Standard contrast-enhanced CT images were acquired for all patients prior to the surgical procedure for radiological evaluation and surgical planning processes. Prior to the surgical procedure, 3-D anatomical models of the liver, tumor(s), and vasculature structures were generated from the preoperative tomograms using surgical planning software (Scout[TM]Liver, Analogic Corporation, Peabody, MA USA). A summary of the methods used in the preoperative planning software have been provided by Li *et al.*[5] and an evaluation of the clinical impact of the the software has been performed by DuBray *et al.*[6] Upon completion of the processing, the preoperative tomographic data and associated anatomical models were then imported into a surgical navigation system (Explorer[TM]Liver, Analogic Corporation, Peabody, MA USA) for used during the open resection procedure.

2.1.2. Intraoperative Data Collection

After laparotomy and liver mobilization, the anterior liver surface was digitized using both a tracked laser range scanner (LRS) and an optically tracked stylus (shown in Figure 2). The LRS device is used to acquire an initial dense scan of the liver surface within line of sight via the laparotomy incision. Further, a brief apneic period, initialized at end-inspiration, is used to minimize motion artifact in the scan due to respiration. The LRS device used in this study has been characterized by Pheiffer *et al.*[7]
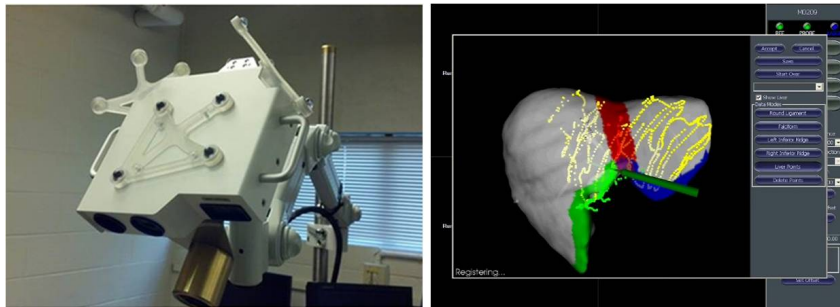

Figure 2. The tracked laser range scanner (LRS) device used for organ surface acquisition during the study (left). The manual surface swabbing interface within the Explorer[TM]Liver navigation system highlighting a surface alignment generated from the probe-based digitization (right).

In addition to the LRS surface digitization, a surface acquisition also performed via manually swabbing the surface of the organ with an optically tracked stylus. In addition to acquiring the liver surface, a series of anatomical features including the umbilical fissure, falciform ligament, and inferior ridges are also acquired for the purposes of driving the salient feature rigid surface registration used within the Explorer[TM]Liver guidance system.[8,9] As with the LRS acquisition, a brief apneic period was used to compensate for respiratory motion.

After qualitative evaluation of the registration within the guidance display, the clinician proceeded to interrogate the organ with the tracked iUS transducer (shown in Figure 3). The Explorer[TM]Liver navigation system is equipped with a tracked rigid body attachment designed for the Aloka T-probe (Hitachi Aloka Medical Ltd., Wallingford, CT USA). The tracked ultrasound system was calibrated using the method described by Chen *et*

$al.$[10] and clinical experience with the tracked iUS equipped navigation system has been described by Kingham et $al.$[11] During the surgical procedure, the clinician utilized the tracked iUS to image anatomical features that could be reliably identified within the preoperative tomograms. During the interrogation, iUS image screen captures and corresponding tracked locations of the transducer were recorded for retrospective evaluation.
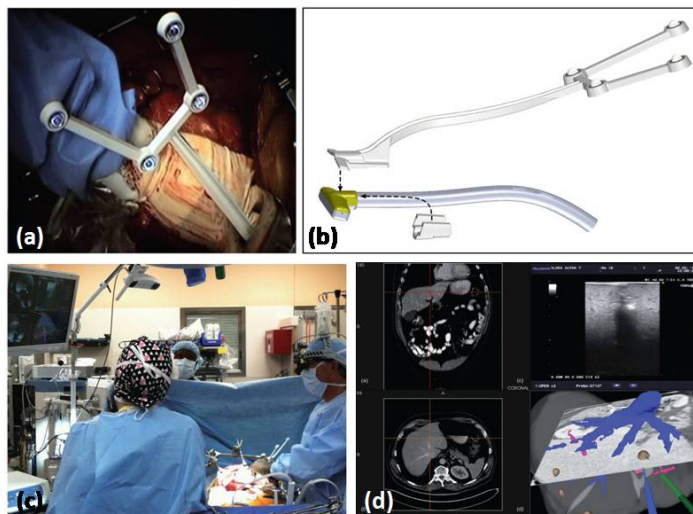

Figure 3. The tracked adapter device in use during surgery during the organ interrogation with ultrasound (a) and a schematic of the adapter used to track an Aloka T-probe (UST-5713-T, Hitachi Aloka Medical Ltd., Wallingford, CT USA) within the Explorer^{TM}Liver navigation system (b). A view of the OR during the use of the tracked iUS functionality within the Explorer^{TM}Liver navigation system (c) and a screen capture of the Explorer^{TM}Liver navigation system with iUS tracking in use during an ablation probe placement in an open hepatic procedure (d). Note that the oblique CT slice that corresponds with the tracked iUS plane is displayed in the lower right quadrant of the interface. These images were published in the work of Kingham et $al.$[11]

2.2. Deformation Correction Method

The deformation correction method that is used for validation in this study has been described by Rucker et $al.$[12] To provide an overview, the method is driven by sparse surface data of the organ collected intraoperatively and utilizes a parameterized "support surface" to reflect the impact of the liver mobilization and "packing" procedure that occurs after laparotomy. The support surface is described by a bivariate polynomial which specifies a series of surface displacements. An optimization framework is then used to determine the optimal parameters for the support surface such that the residual error between the intraoperative sparse surface digitization and the deformed liver surface, generated from preoperative images, is minimized.

2.2.1. Biomechanical Liver Model

The underlying tissue deformation model begins with the assumption that the liver is an isotropic solid with a linear stress-strain relationship as in previous studies[13–15] where the displacement field can be given by the standard 3-D Navier-Cauchy equations:

$$\frac{E}{2(1+\nu)}\nabla^2\mathbf{u} + \frac{E}{2(1+\nu)(1-2\nu)}\nabla(\nabla \cdot \mathbf{u}) = \mathbf{B} \tag{1}$$

where E is Young's Modulus, ν is Poisson's ratio, $\mathbf{u}$ is the 3-D displacement vector and $\mathbf{B}$ is the body force distribution. In order to solve the system equations in Equation 1 over the liver mesh domain, the Galerkin weighted residual method is applied using linear basis functions. Using this technique, the system of partial differential equations reflecting the displacement vectors ($\mathbf{u}$) at each node in the tetrahedral mesh can be compiled in matrix form using the following relation:

$$[K]\{\mathbf{u}\} = \{\mathbf{b}\} \tag{2}$$

where $[K]$ is the global stiffness matrix and $\{\mathbf{b}\}$ is the body force distribution at each mesh node. The driving force behind generating deformations with an FEM model is provided by the prescription of the appropriate conditions along the boundary of the tetrahedral mesh.

2.2.2. Nonrigid Deformation and Optimization Algorithm

As mentioned, the Dirichlet boundary conditions are determined by a "support surface" specified to the posterior region of the organ surface. The support surface is specified via the bivariate polynomial form as follows:

$$\mathbf{u}_s = \hat{\mathbf{n}}_s \sum_{1 \leq i+j \leq n} c_{ij} t_1^i t_2^j \tag{3}$$

where $\mathbf{u}_s$ is the displacement vector for a point on the support surface, $\hat{\mathbf{n}}_s$ is the average normal unit vector over the designated support region (the area weighted average over the triangular boundary elements), and t_1 and t_2 are the tangential coordinates of the point on the support surface (measured from the origin perpendicular to $\hat{\mathbf{n}}_s$ in two orthogonal directions). Thus, the constant coefficients c_{ij} define the nonrigid displacement field over the support region. The sum over $1 \leq i + j \leq n$ avoids redundancy with the subsequent rigid transformation by excluding the constant displacement mode, which is captured with general rigid body motion.

Using the principle of superposition, it is possible to facilitate rapid computation of model solutions given a combination of support surface coefficients. The model solution for each of the coefficients c_{ij} is pre-computed and stored in matrix $[M]$, where each column is the displacement vector u_{ij} obtain by solving Eq. 2 where the right-hand side vector is computed with $c_{ij} = 1$ with all other coefficients set to zero. Therefore, the following equation can be used for rapid model solution computation:

$$\{\mathbf{u}\} = [M]\{\mathbf{c}\} \tag{4}$$

where $\{\mathbf{c}\} = [c_{01}, c_{10}, c_{02}, c_{11}, c_{20}...c_{n0}]^T$ and $\{\mathbf{u}\}$ is the vector of node displacements.

After generating a model solution for a particular set of polynomial coefficients, the rigid alignment can be updated between the intraoperative surface digitization and the deformed organ model. To achieve this end, a six degree-of-freedom rigid body transformation cam be applied to the deformed nodal coordinates. Therefore, the set of parameters used to generate the total displacement field is as follows:

$$\mathbf{P} = \left\{ \mathbf{c}^T, t_x, t_y, t_z, \theta_x, \theta_y, \theta_z \right\} \tag{5}$$

The optimal parameter set in Eq. 5 is determined via a Levenberg-Marquardt algorithm such that the following objective function is minimized:

$$F = \frac{1}{N} \sum_{i=1}^{N} \left(\hat{\mathbf{n}}_{ci}^T \left(\mathbf{p}_{di} - \mathbf{p}_{ci} \right) \right)^2 + \alpha E^2 \tag{6}$$

where $\mathbf{p}_{di}$ is a 3×1 vector containing the Cartesian coordinates for the location of the ith point in the intraoperative sparse surface, $\mathbf{p}_{ci}$ is the location of the corresponding point on the preoperative organ model surface, generated via the closest point operator, and $\hat{\mathbf{n}}_{ci}$ is a unit vector normal to the model surface at $\mathbf{p}_{ci}$. E is proportional to the total strain energy stored in the displacement field produced by the model solution and is calculated as $E = \{\mathbf{u}\}^T [K] \{\mathbf{u}\}$. Given that α is a weighting constant, the term αE serves as a regularization term for the optimization to balance the distortion of the deformation field.

To summarize the method, a flowchart representation of the deformation correction algorithm is provided in Figure 4. The algorithm is initialized via initial rigid surface alignment between the intraoperative surface digitization and preoperative organ model. The optimization procedure is performed for a fixed number of iterations or until the residual error between the two surfaces reaches a certain threshold.
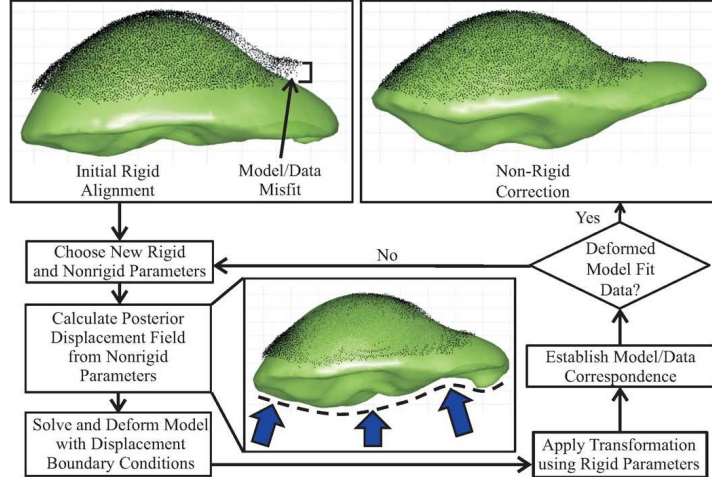
Figure 4. Schematic of the deformation correction algorithm for model-updated image-guided liver surgery (published in Rucker *et al.*[12]). The algorithm is driven by sparse data acquisition of the liver surface and is based on a linear elastic model of the liver tissue and the premise that a support surface can represent boundary displacements imposed during the surgical procedure. Parameters are updated via a nonlinear optimization routine. In this work, we used the Levenberg-Marquardt algorithm where the required gradients were computed via forward finite differences.

2.3. Retrospective Validation Procedure

Using the liver surface generated from the preoperative tomograms, a tetrahedral mesh of the organ was generated using a customized mesh generator. We employ the algorithm described by Sullivan *et al.* to generate the tetrahedral liver mesh. After mesh generation, a "support surface" region on the posterior side of the organ is delineated for the non-rigid correction algorithm.[16] The mechanics-based correction algorithm was initialized with the rigid surface registration computed within the Explorer^{TM}Liver guidance system,[9] and the final solution of mesh node displacements was used to deform the 3-D surface models of the patient anatomy generated from the preoperative tomograms. As in the work of Rucker *et al.*, the values for the non-rigid correction parameters used in this work were as follows: Young's modulus (E) of 2100 Pa, Poisson's ratio (ν) of 0.45, and energy weighting coefficient (α) of 2×10^{-4}.[12] It should be noted that the intraoperative surface digitizations acquired from the tracked LRS device and the tracked stylus were concatenated to maximize the extent of organ coverage for the deformation correction algorithm.

Upon completion of the surgical procedure, a review of the tracked iUS images acquired was performed by the clinician to delineate anatomical structures that would best serve as targets for the deformation correction evaluation. Based on the clinician review, contour segmentations were performed of the anatomical structures (i.e. vessels) and transformed by both the rigid surface registration computed within the guidance system and the updated rigid surface registration computed within the deformation correction algorithm. The quantitative error metric used was the mean closest point distance between the contours segmented in the iUS images and the corresponding 3-D models of the structures generated from the preoperative tomograms. To clarify, the deformed anatomical models were used for the contour-to-model closest point distance calculation for the deformation correction evaluation.

3. RESULTS

A qualitative visualization is shown to represent the impact of the deformation correction algorithm on the alignment of the tracked iUS with the corresponding anatomical feature generated from the preoperative tomograms. Figure 5 depicts a rendering of the alignment of a tracked iUS image of the right hepatic vein under conditions of rigid registration and deformation correction for Patient 2. It should be noted that the visualization of the result of the deformation correction involves both the deformed anatomical models and an updated rigid body

Patient	Anatomical Feature	Rigid Registration Error (mm)	Post-Correction Error (mm)	Mean Shift Correction (%)
1	Left Portal Vein Confluence	4.9 ± 3.1 (10.0)	2.0 ± 1.2 (4.9)	59.2
2	Right Hepatic Vein	4.6 ± 2.8 (11.3)	2.0 ± 1.3 (5.4)	56.5

Table 1. A summary of the contour-to-model closet point distance errors between homologous features delineated in the preoperative tomograms and the tracked iUS image sets under conditions of rigid registration and post-deformation correction. The maximum contour-to-model closest point distance is shown in parentheses. A mean shift correction measurement is also presented for each feature to provide a sense of the efficacy of the model-based correction algorithm.

transform. Qualitatively, the alignment between the iUS image of the vascular structure and the preoperative model is substantially improved by the deformation correction algorithm.
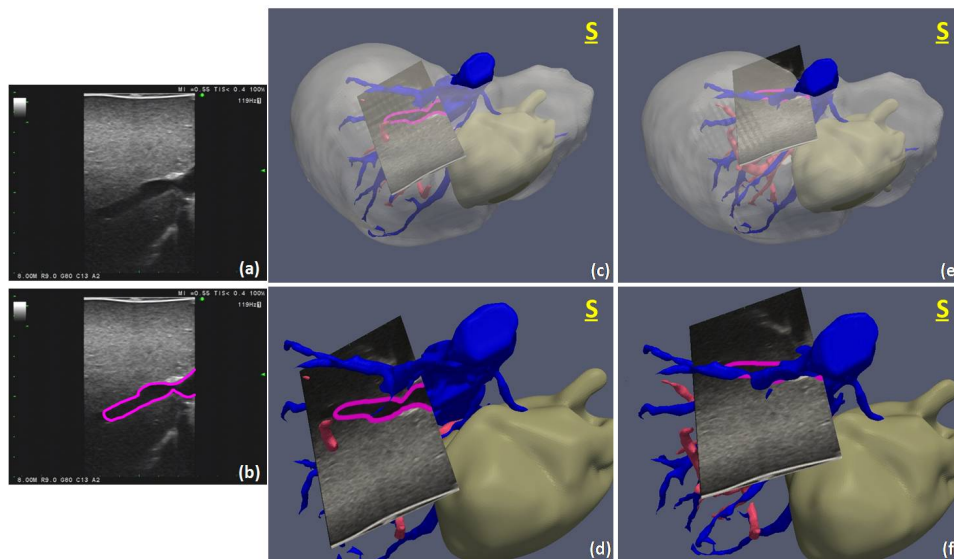

Figure 5. Visualization of the tracked iUS image plane rendered within the 3-D models generated from the preoperative tomograms for Patient 2. The raw iUS image captures used in the analysis are shown in panel (a) and panel (b) shows the highlighted anatomical feature (i.e. right hepatic vein). The rigid registration transformation computed during the surgical procedure was used to generate the overlays in panels (c) and (d). Panel (c) depicts a superior view of the rigid alignment and includes a rendering of the lesion (brown), portal vasculature (pink), hepatic vasculature (blue) and liver surface (grey). Panel (d) depicts a zoomed superior view of the tracked iUS and hepatic vein structure. The deformed anatomical models and updated transform from the deformation correction algorithm were used to generate the renderings in panels (e) and (f). Panel (e) depicts a superior view of the deformation corrected alignment and includes a rendering of the lesion (brown), portal vasculature (pink), hepatic vasculature (blue) and liver surface (grey). Panel (f) depicts a zoomed superior view of the tracked iUS and hepatic vein structure after deformation correction.

A summary of the contour-to-model closest point distance measurements for the anatomical sub-surface targets for the two clinical cases is shown in Table 1. As shown, the deformation correction method appears to improve registration accuracy by approximately 50% as implied by the qualitative improvement in the iUS alignment highlighted in the visualization in Figure 5.

4. DISCUSSION

The results presented represent the first effort to validate a biomechanical model-base deformation correction algorithm for IGLS driven by sparse surface data using clinically acquired sub-surface anatomical targets. It should be noted that previous work by Lange *et al.* has employed a validation technique using clinical data for

their spline-based deformation correction algorithm.[17] The work presented here is differentiated due to the fact that the the sub-surface anatomical targets used in the algorithm validation were completely segregated from the sparse data used to drive the model. In other words, the model-based deformation correction algorithm employed in this work was driven solely by sparse surface data acquired intraoperatively, while the validation metrics were computed using sub-surface anatomical targets digitized via tracked iUS.

The visualization (shown in Figure 5) of the impact of the deformation correction algorithm on tracked iUS alignment indicates that the proposed algorithm provides a substantial correction for the soft tissue deformation encountered during these procedures. Additionally, the quantitative summary of the sub-surface contour-to-surface distance errors indicates that the correction algorithm can compensate for approximately 50% of the encounter soft tissue shift. In summary, the clinical validation presented within the evaluation of previously proposed deformation correction techniques for open liver image-guidance have largely relied on surface-based metrics and phantom experiments have been used for the characterization of sub-surface target accuracy. The proposed method represents a significant advancement in methodology for the validation of deformation correction in open hepatic surgical navigation via the use of independent sub-surface anatomical targets acquired during clinical procedures for validation.

5. CONCLUSION

The preliminary results indicate that the proposed validation method is promising in facilitating the refinement of deformation correction algorithms for image-guidance systems used in open liver procedures. Future work will involve the generation of 3-D models of the anatomical structures acquired via the tracked iUS framework to facilitate the computation of more descriptive target error metrics. Additionally, a more extensive array of deformation correction algorithms will be evaluated retrospectively using the tracked iUS dataset being acquired in the ongoing clinical study at Memorial Sloan-Kettering Cancer Center.

ACKNOWLEDGMENTS

REFERENCES

1. O. Heizmann, S. Zidowitz, H. Bourquain, S. Potthast, H.-O. Peitgen, D. Oertli, and C. Kettelhack, "Assessment of intraoperative liver deformation during hepatic resection: prospective clinical study.," *World J Surg* **34**, pp. 1887–1893, Aug 2010.

2. D. M. Cash, S. C. Glasgow, L. W. Clements, M. I. Miga, B. Dawant, Z. Cao, R. L. Galloway, and W. C. Chapman, "Concepts and preliminary data towards the realization of an image-guided liver surgery system," *J Gastrointest Surg* **11**, pp. 844–59, July 2007.

3. L. Clements, P. Dumpuri, W. Chapman, B. Dawant, R. Galloway, and M. Miga, "Organ surface deformation measurement and analysis in open hepatic surgery: method and preliminary results from 12 clinical cases.," *IEEE Trans Biomed Eng* , Apr 2011.

4. S. Beller, M. Hnerbein, S. Eulenstein, T. Lange, and P. M. Schlag, "Feasibility of navigated resection of liver tumors using multiplanar visualization of intraoperative 3-dimensional ultrasound data.," *Ann Surg* **246**, pp. 288–294, Aug 2007.

5. S. Li, J. M. Waite, B. T. Lennon, J. D. Stefansic, R. Li, and B. M. Dawant, "Development of preoperative liver and vascular system segmentation and modeling tool for image-guided surgery and surgical planning," 2008.

6. B. J. DuBray, R. V. Levy, P. Balachandran, K. D. Conzen, G. A. Upadhya, C. D. Anderson, and W. C. Chapman, "Novel three-dimensional imaging technique improves the accuracy of hepatic volumetric assessment.," *HPB (Oxford)* **13**, pp. 670–674, Sep 2011.

7. T. S. Pheiffer, A. L. Simpson, B. Lennon, R. C. Thompson, and M. I. Miga, "Design and evaluation of an optically-tracked single-ccd laser range scanner.," *Med Phys* **39**, pp. 636–642, Feb 2012.

8. L. Clements, D. Cash, W. Chapman, R. Galloway Jr., and M. Miga, "Robust surface registration using salient anatomical features in image-guided liver surgery," in *SPIE 2006 Medical Imaging: Visualization, Image-Guided Procedures, and Display,* **6141**, pp. 105–115, 2006.

9. L. W. Clements, W. C. Chapman, B. M. Dawant, R. L. Galloway, and M. I. Miga, "Robust surface registration using salient anatomical features for image-guided liver surgery: algorithm and validation.," *Med Phys* **35**, pp. 2528–2540, Jun 2008.

10. T. K. Chen, A. D. Thurston, R. E. Ellis, and P. Abolmaesumi, "A real-time freehand ultrasound calibration system with automatic accuracy feedback and control.," *Ultrasound Med Biol* **35**, pp. 79–93, Jan 2009.

11. T. P. Kingham, M. A. Scherer, B. W. Neese, L. W. Clements, J. D. Stefansic, and W. R. Jarnagin, "Image-guided liver surgery: intraoperative projection of computed tomography images utilizing tracked ultrasound.," *HPB (Oxford)* **14**, pp. 594–603, Sep 2012.

12. D. Rucker, Y. Wu, L. Clements, J. Ondrake, T. Pheiffer, A. Simpson, W. Jarnagin, and M. Miga, "A mechanics-based nonrigid registration method for liver surgery using sparse intraoperative data.," *IEEE Trans Med Imaging* , Sep 2013.

13. M. Miga, D. Cash, Z. Cao, G. R.L., B. Dawant, and W. Chapman, "Intraoperative registration of the liver for image-guided surgery using laser range scanning and deformable models," *SPIE Medical Imaging 2003* **5029**, 2003.

14. D. M. Cash, M. I. Miga, T. K. Sinha, R. L. Galloway, and W. C. Chapman, "Compensating for intraoperative soft-tissue deformations using incomplete surface data and finite elements," *IEEE Trans. Med. Imaging* **24**, pp. 1479–1491, Nov. 2005.

15. P. Dumpuri, L. W. Clements, B. M. Dawant, and M. I. Miga, "Model-updated image-guided liver surgery: preliminary results using surface characterization.," *Prog Biophys Mol Biol* **103**, pp. 197–207, Dec 2010.

16. J. Sullivan, G. Charron, and K. Paulsen, "A three-dimensional mesh generator for arbitrary multiple material domains," *Finite Elements in Analysis and Design* **25**(3-4), pp. 219–241, 1997.

17. T. Lange, N. Papenberg, S. Heldmann, J. Modersitzki, B. Fischer, H. Lamecker, and P. M. Schlag, "3d ultrasound-ct registration of the liver using combined landmark-intensity information.," *Int J Comput Assist Radiol Surg* **4**, pp. 79–88, Jan 2009.